Electronic Supplementary Information

Interfacial synthesis of ordered and stable covalent organic framework on amino-functionalized carbon nanotube with enhanced electrochemical performance

Bing Sun,‡[a, b] Jian Liu,‡[a, b] Anmin Cao,[a] Weiguo Song,[a] and Dong Wang,*[a,b]

[a] Key Laboratory of Molecular Nanostructure and Nanotechnology and Beijing National Laboratory for Molecular Sciences, Institute of Chemistry, Chinese Academy of Sciences (CAS), Beijing 100190, P. R. China

[b] University of CAS, Beijing 100049, P. R. China

Corresponding Author:

*E-mail: wangd@iccas.ac.cn; Tel: +86-10-82616953

‡ These authors contribute equally to this work.

S1. Experimental details

Synthesis of COF$_{TTA\text{-}DHTA}$ powders

4,4',4''-(1,3,5-triazine-2,4,6-triyl)trianiline (TTA) and 2,5-dihydroxyterethaldehyde (DHTA) were synthesized from 4-nitrobenzonitrile and 1,4-dimethoxy-benzen, respectively, according to previous reported procedures.[1, 2] Their ^{1}H NMR and ^{13}C NMR spectra were consistent well with that in the related literatures. A mixture of TTA (35.4 mg, 0.1 mmol), DHTA (24.9 mg, 0.15 mmol), dioxane (2 mL) and mesitylene (1 mL) was charged in a cylindrical glass tube (18 cm of length, ϕ_{in} = 0.8 cm, ϕ_{out} = 1.0 cm) and sonicated for 15 minutes to get a homogenous dispersion. Then 0.2 mL of 6 M aqueous acetic acid was dropwise added to the mixture, along with the color changed from yellow to brick-red. After degased by the typical three freeze-pump-thaw cycles, the tube was sealed off and then heated at 120 °C for 3 days. The red precipitate was collected by filtration and rinsed with *N*,*N*-dimethylformylamide (DMF) and tetrahydrofuran (THF) in turn. The powders were steepened in the mixed solvent of THF and dichloroethane (1:1 in v/v) to exchange for 8 h, and then collected and dried at 120 °C for 24 h.

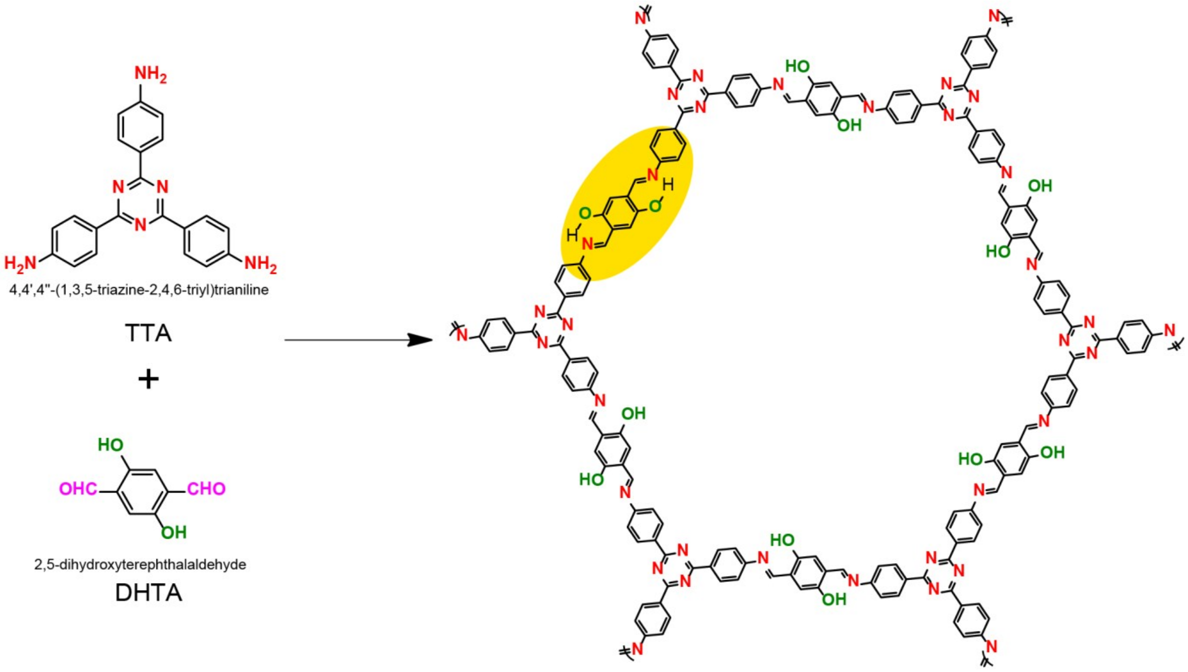

Scheme S1. Synthesis of COF$_{TTA\text{-}DHTA}$ from TTA and DHTA.

Synthesis of NH_2-f-MWCNT@$COF_{TTA\text{-}DHTA}$ and MWCNT@$COF_{TTA\text{-}DHTA}$

In a typical procedure, DHTA (5.1 mg, 0.03 mmol) was dissolved in 1 mL of amino-functionalized multi-walled carbon nanotube (NH_2-f-MWCNT, purity more than 95%, -NH_2 content：0.45 wt%, Chengdu Organic Chemicals CO., LTD, Chinese Academy of Sciences) homogeneous suspension (5, 10, 20 mg mL^{-1} in dioxane/mesitylene/DMF, 2:1:0.2 in v/v, which were obtained by suspending constant amount of NH_2-f-MWCNT in dioxane/mesitylene/DMF and sheared stirring overnight.) charged in a cylindrical glass tube (18 cm of length, $\phi_{in} = 0.8$ cm, $\phi_{out} =$ 1.0 cm). The mixture was stirred for 1 h, then, TTA (7.1 mg, 0.02 mmol) dispersed in 1 mL of dioxane/mesitylene (2:1 in v/v) and 0.1 mL of 6 M aqueous acetic acid were successively added in 1 h. After stirred for another 1 h and the typical three freeze-pump-thaw cycles, the tube was sealed off and heated at 120 °C for a certain time. The products denoted as NH_2-f-MWCNT@$COF_{TTA\text{-}DHTA}$ were collected and treated in a similar procedure with that for $COF_{TTA\text{-}DHTA}$ powders. MWCNT@$COF_{TTA\text{-}DHTA}$ was also synthesized in the same method.

General characterization methods

Powder X-ray diffraction (PXRD) patterns were recorded on a PANalytical Empyrean Diffractometer operated at 40 kV and 40 mA with Cu Kα radiation ($\lambda = 1.5416$ Å) ranging from 1.5 to 50° with a speed of 2 °/min at ambient temperature. FT-IR spectra were recorded with a Bruker RFS100/S instrument in the range of 400 to 4000 cm^{-1} with an interval of 4 cm^{-1}. Morphology observation was performed using JEM-2100F transmission electron microscopy at an accelerating voltage of 200 kV. The TEM Samples were prepared by dropping the sample from anhydrous ethanol on copper grids supporting a thin, electron transparent carbon film. Nitrogen adsorption and desorption isotherms were measured using Micromeritics ASAP-2020 Surface Area and Porosity Analyzer. The samples loaded in sample tubes were heated to 90 °C under a vacuum of 0.5 mtorr for 24 h, and the measurements were conducted at liquid nitrogen temperature (77 K) using ultrahigh-purity grade nitrogen (99.999%).

Electrochemical measurements

All the electrochemical measurements were performed on a Metrohm Autolab PGSTA302A electrochemical station with a standard three-electrode system at 25 °C in 1 M Na_2SO_4 (Sigma-Aldrich) aqueous solution. An Ag/AgCl (saturated KCl) electrode and platinum foil (1×1 cm^2) were used as the reference and counter electrodes, respectively. The working electrode was fabricated as followed. A powder sample (NH_2-f-MWCNT@$COF_{TTA\text{-}DHTA}$, MWCNT@$COF_{TTA\text{-}DHTA}$ or $COF_{TTA\text{-}DHTA}$), PVDF (5 wt%, Kynar®, Arkema) as the binder and Super P® conductive carbon (TIMCAL Graphite & Carbon) were mixed thoroughly in a weight ratio of 80:10:10, and then were coated onto a foamed nickel (in 1×1 cm^2). The electrolyte was purified with ultrahigh pure argon for 0.5 h and kept at argon atmosphere in the measurement procedure. Cyclic voltammetry measurements were performed in the potential window of 0 – 0.8 V under various scan rates. The galvanostatic charge-discharge were tested at different constant current density and the charge/discharge potential−time curve was used to calculate capacitances based on $C = i\ \Delta t/\Delta V$, where C (A g^{-1}) is specific capacitance, i (A g^{-1}) represents charge/discharge current density, ΔV (V) represents the potential change during charge/discharge, Δt (s) is the total charge/discharge time.

S2. Synthesis and characterization of $COF_{TTA\text{-}DHTA}$

Table S1. Fractional atomic coordinates for the unit cell of $COF_{TTA\text{-}DHTA}$ (Eclipsed) by using the self-consistent charge density functional tight-binding (SCC-DFTB) method.[3]

$a = b = 36.13$ Å, $c = 3.49$ Å, $\alpha = \beta = 90°$, $\gamma = 120°$

Atom	No.	x	y	z	Atom	No.	x	y	z
H	1	1.974412	-0.448335	0.822448	H	40	1.093291	-0.483382	0.684069
H	2	1.907315	-0.498932	0.738137	H	41	1.026185	-0.533979	0.597685
H	3	1.837878	-0.522553	0.719494	H	42	1.07225	-0.404914	0.968453
H	4	1.768071	-0.553744	0.721882	C	1	1.984771	-0.467964	0.768985
H	5	1.759205	-0.665271	0.689532	C	2	1.957696	-0.508049	0.707226
H	6	1.828294	-0.63403	0.686111	C	3	1.975342	-0.530819	0.64285
H	7	1.928337	-0.577411	0.451865	C	4	1.913322	-0.522253	0.713031
H	8	1.670022	-0.754125	0.7162	C	5	1.840822	-0.574988	0.70308
H	9	1.630305	-0.825967	0.716736	C	6	1.821377	-0.553708	0.713116
H	10	1.53182	-0.815698	0.699283	C	7	1.780373	-0.572143	0.714206
H	11	1.570748	-0.744598	0.699468	C	8	1.755358	-0.613323	0.706046
H	12	1.678504	-0.551366	0.700659	C	9	1.775323	-0.634035	0.696511
H	13	1.645047	-0.514358	0.70025	C	10	1.815911	-0.615739	0.694598
H	14	1.539468	-0.619391	0.715809	C	11	1.709959	-0.634759	0.707123
H	15	1.572777	-0.656991	0.715636	C	12	1.651558	-0.632495	0.708053
H	16	1.513183	-0.575439	0.719545	C	13	1.649353	-0.694664	0.707763
H	17	1.53745	-0.420978	0.711679	C	14	1.624845	-0.7411	0.707825
H	18	1.46035	-0.562555	0.713862	C	15	1.639854	-0.766753	0.712436
H	19	1.484613	-0.408099	0.719624	C	16	1.616694	-0.808837	0.712781
H	20	1.458341	-0.364159	0.716848	C	17	1.576654	-0.828531	0.70805
H	21	1.42505	-0.326544	0.717328	C	18	1.561965	-0.802979	0.703192
H	22	1.319303	-0.432148	0.703495	C	19	1.584832	-0.761328	0.703303
H	23	1.352745	-0.469175	0.70246	C	20	1.629624	-0.608457	0.708203
H	24	1.409581	-0.513095	0.826788	C	21	1.648155	-0.56726	0.704071
H	25	1.588298	-0.470412	0.821236	C	22	1.628572	-0.545532	0.70382
H	26	1.232538	-0.428467	0.705202	C	23	1.588725	-0.562642	0.708038
H	27	1.162804	-0.459653	0.70717	C	24	1.56976	-0.603855	0.71237
H	28	1.172173	-0.348265	0.725773	C	25	1.589434	-0.625787	0.712253
H	29	1.241142	-0.316872	0.722488	C	26	1.534557	-0.54527	0.714134
H	30	1.427183	-0.238892	0.700979	C	27	1.518048	-0.516131	0.714068
H	31	1.466128	-0.167791	0.699587	C	28	1.538338	-0.474608	0.717909
H	32	1.36767	-0.157486	0.721673	C	29	1.519632	-0.451984	0.711466
H	33	1.327938	-0.229325	0.722366	C	30	1.479755	-0.467402	0.71445
H	34	1.413642	-0.087007	0.724984	C	31	1.459467	-0.508921	0.719513
H	35	1.430759	-0.01819	0.71648	C	32	1.478169	-0.531549	0.712612
H	36	1.51343	-0.066296	0.849456	C	33	1.463241	-0.43827	0.714762
H	37	1.584339	-0.896456	0.721442	C	34	1.409074	-0.420901	0.709585
H	38	1.56722	-0.965278	0.712801	C	35	1.428049	-0.379688	0.713773
H	39	1.484608	-0.917164	0.851756	C	36	1.408385	-0.357748	0.714026

Atom	No.	x	y	z	Atom	No.	x	y	z
C	37	1.368196	-0.375065	0.710497	C	61	1.537415	-0.975899	0.712673
C	38	1.349653	-0.416264	0.706477	C	62	1.484903	-0.965999	0.722329
C	39	1.369227	-0.438002	0.705874	C	63	1.087273	-0.460058	0.707523
C	40	1.346287	-0.351004	0.711056	C	64	1.042898	-0.474264	0.712807
C	41	1.348571	-0.288801	0.712288	C	65	1.015825	-0.514349	0.65105
C	42	1.287895	-0.348681	0.712678	C	66	1.025253	-0.451494	0.777139
C	43	1.245293	-0.368775	0.713525	N	1	1.883308	-0.558422	0.697946
C	44	1.220283	-0.410011	0.70939	N	2	1.69059	-0.614462	0.707639
C	45	1.179271	-0.428491	0.710218	N	3	1.632059	-0.672507	0.708116
C	46	1.159767	-0.407265	0.716067	N	4	1.688307	-0.674867	0.707154
C	47	1.184615	-0.366509	0.720639	N	5	1.550261	-0.872046	0.708182
C	48	1.225202	-0.348128	0.71882	N	6	1.570514	-0.537477	0.707834
C	49	1.3731	-0.242368	0.711842	N	7	1.427281	-0.44607	0.70912
C	50	1.41311	-0.222153	0.705651	N	8	1.365825	-0.310992	0.711338
C	51	1.435986	-0.180502	0.70482	N	9	1.309625	-0.30856	0.713315
C	52	1.421309	-0.15494	0.710534	N	10	1.307252	-0.369007	0.71136
C	53	1.381271	-0.174623	0.716954	N	11	1.447708	-0.111426	0.709711
C	54	1.358104	-0.216705	0.717338	N	12	1.117275	-0.423874	0.720989
C	55	1.442385	-0.080761	0.717657	O	1	1.954001	-0.57007	0.555892
C	56	1.472925	-0.035365	0.716805	O	2	1.420424	-0.529565	0.740053
C	57	1.51308	-0.017468	0.721146	O	3	1.577391	-0.453948	0.736509
C	58	1.460564	-0.007569	0.714695	O	4	1.530607	-0.039548	0.744373
C	59	1.555592	-0.902707	0.715579	O	5	1.467389	-0.943915	0.746958
C	60	1.525054	-0.948103	0.71588	O	6	1.046594	-0.412246	0.864218

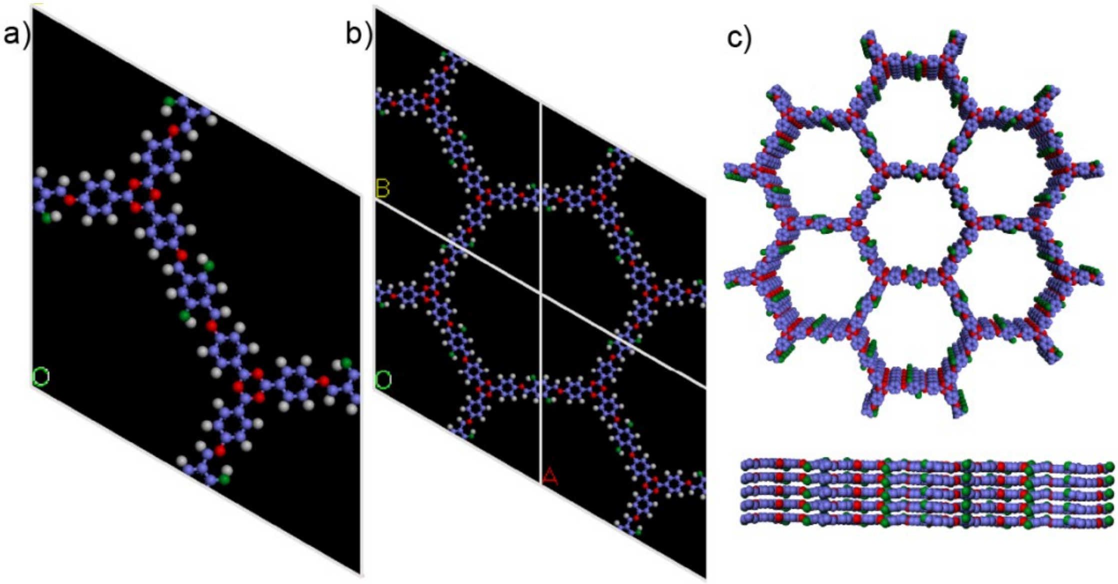

Fig. S1 (a) Unit cell and (b) eclipsed crystal lattice packing of $COF_{TTA\text{-}DHTA}$. (c) Graphic top-view and layered view of $COF_{TTA\text{-}DHTA}$ (red, N; violet, C; olive, O; hydrogen is omitted for clarity)

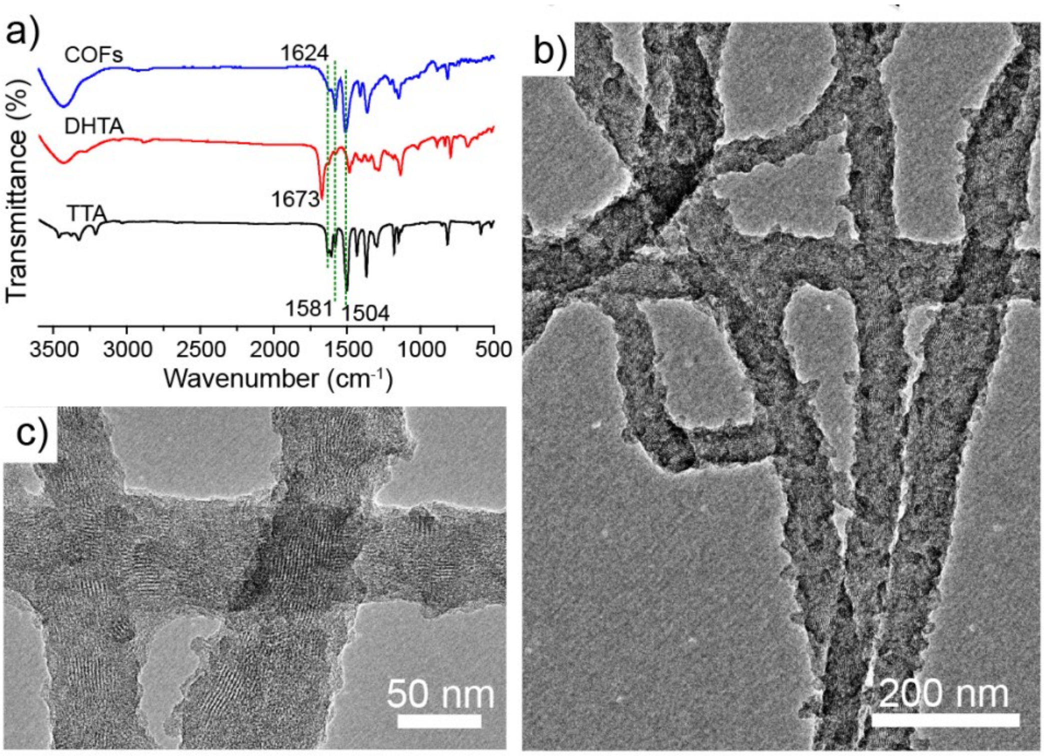

Fig. S2 (a) FTIR spectra of $COF_{TTA\text{-}DHTA}$ comparing with the monomers TTA and DHTA. (b, c) TEM image of $COF_{TTA\text{-}DHTA}$ in different magnified scales.

Fourier transform infrared (FT-IR) spectra of $COF_{TTA\text{-}DHTA}$ shown in Fig. S2a are utilized to confirm the formation of imine structure in $COF_{TTA\text{-}DHTA}$. By comparing the FT-IR spectrum of $COF_{TTA\text{-}DHTA}$ with that of the corresponding monomers, the disappearance of the characteristic N-H stretching bands around 3200 – 3500 cm^{-1} of TTA and C=O stretching band at 1673 cm^{-1} of DHTA indicates the complete consumption of starting materials. The FT-IR peak at 1624 cm^{-1} reveals the formation of imine bond which corresponds to the –C=N– stretching vibration mode. Transmission electron microscopy (TEM) images of $COF_{TTA\text{-}DHTA}$ show the morphology of ribbon-shape crystallites with the diameter in the range of 50 – 90 nm and several micrometers in length (Fig. S2b). The length-diameter ratio can be evaluated as 37.5 ± 12. The distinct and ordered channels with a pore size of about 3.3 nm are observed to parallel the ribbon length direction.

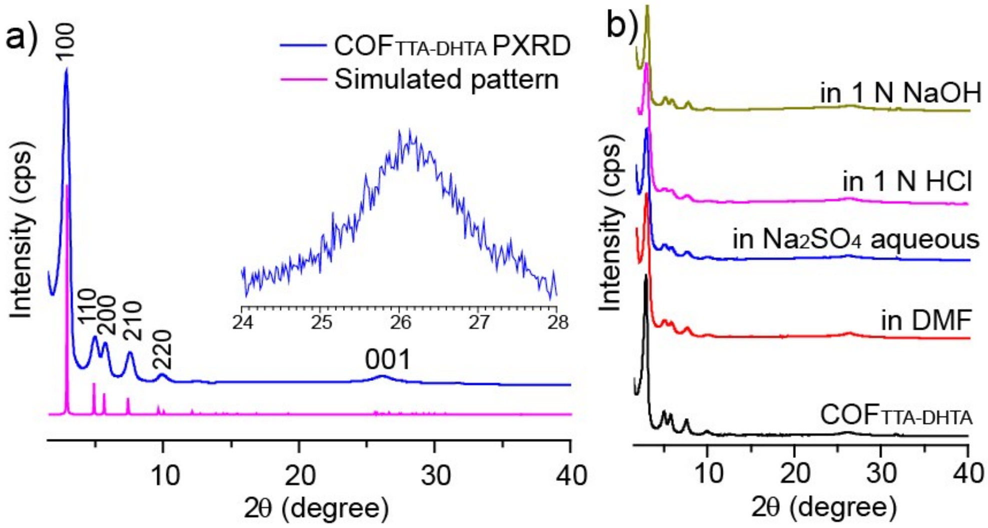

Fig. S3 (a) Experimental PXRD pattern (blue curve) compared with simulated pattern in eclipsed conformation (magenta curve). Inset: magnified scale in the range of 24 to 28° corresponding to (001) facet. (b) PXRD patterns showing the stability of $\mathrm{COF_{TTA\text{-}DHTA}}$ in different solvents for 7 days.

PXRD pattern of $\mathrm{COF_{TTA\text{-}DHTA}}$ reveals its good crystallinity (Fig. S3a). The highly intense peak at 2.77° is corresponding to the (100) plane reflections. Four other prominent peaks at 4.90°, 5.69°, 7.52° and 9.89° are assigned to (110), (200), (210), and (220) facets, respectively. Particularly, the remarkable peak at 26.14° is ascribed to (001) planes (Fig. S3a, inset) and the π-π stacking distance is calculated to be about 3.4 Å from the *d* spacing distance between the (001) facets. The experimental PXRD pattern is well consistent with the simulated pattern of the eclipsed stacking model (Fig. S1). Based on the experimental data, the unit cell values of $\mathrm{COF_{TTA\text{-}DHTA}}$ are calculated as $a = b = 33.29$ Å, $c = 3.41$ Å, which matches well with the simulated unit cell parameters of $a = b = 36.13$ Å, $c= 3.49$ Å with enhanced molecular reactions (Table S1 and Fig. S1). The intensity ratio of 100/001 planes is 41.4 (Fig. S3a). It indicates the strong π-π stacking interaction between each planar conjugated layers and the preferential growth along *c*-axis compared to *a* or *b* directions.[1]

The chemical stability of $\mathrm{COF_{TTA\text{-}DHTA}}$ was investigated by submerging $\mathrm{COF_{TTA\text{-}DHTA}}$ powders in various solvents for a week. As shown in Fig. S3b, PXRD profiles of the residual powders from dimethylformamide (DMF), Na_2SO_4 aqueous solution (1 M), HCl (1 M) and NaOH (1 M) display the high intensities and unchanged peak positions. It suggests that the $\mathrm{COF_{TTA\text{-}DHTA}}$ retains its original crystalline structure and shows the chemical stability in acid, alkali and aqueous solutions.

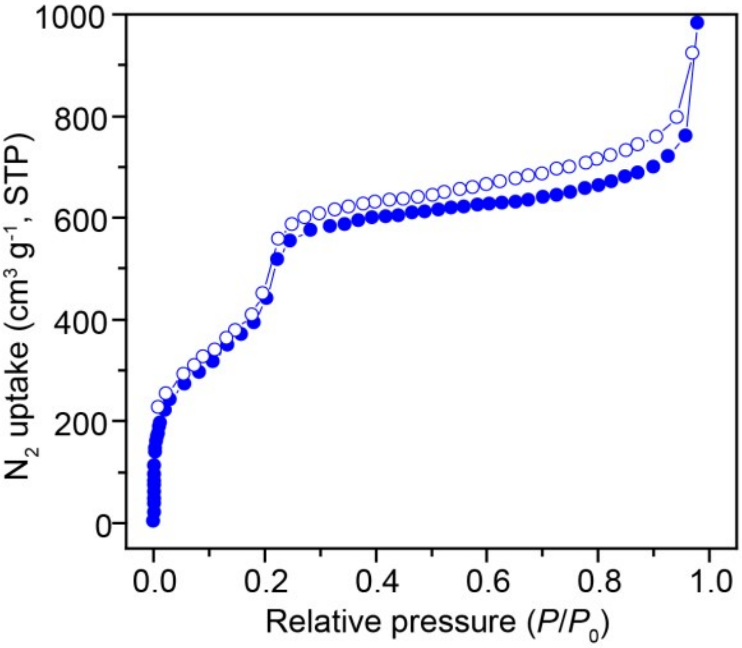

Fig. S4 Nitrogen adsorption-desorption isotherms at 77 K for $COF_{TTA-DHTA}$ powders.

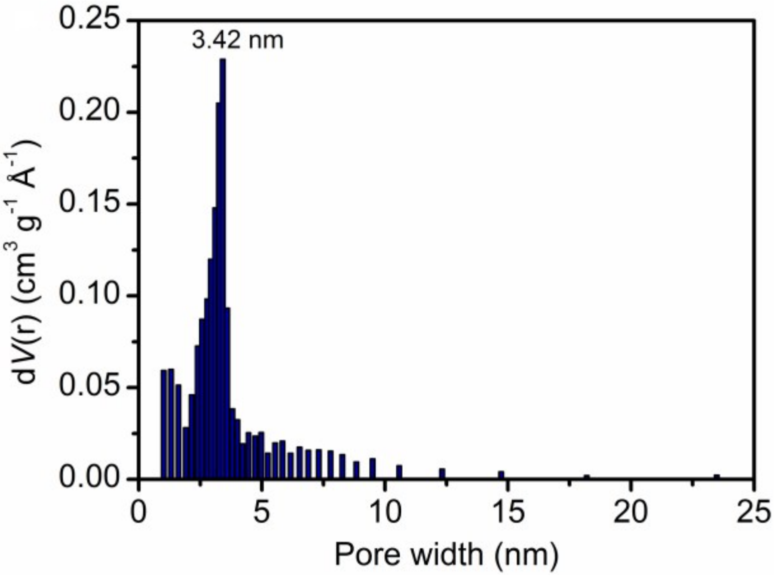

Fig. S5 Pore size distribution of $COF_{TTA-DHTA}$.

For $COF_{TTA-DHTA}$ powder, the reversible type-IV isotherm (Fig. S7) demonstrates its mesoporous characteristic. The surface area is calculated to be 1591 m^2 g^{-1} by using Brunauer-Emmett-Teller (BET) model. Pore distribution evaluated based on nonlocal density functional theory (NLDFT, Fig. S5) shows the main pore size of 3.42 nm which is close to the calculated value (3.6 nm) and PXRD data (3.33 nm) (Fig. S1 and S3).

S3. Further characterizations of NH_2-f-MWCNT@COF$_{TTA\text{-}DHTA}$

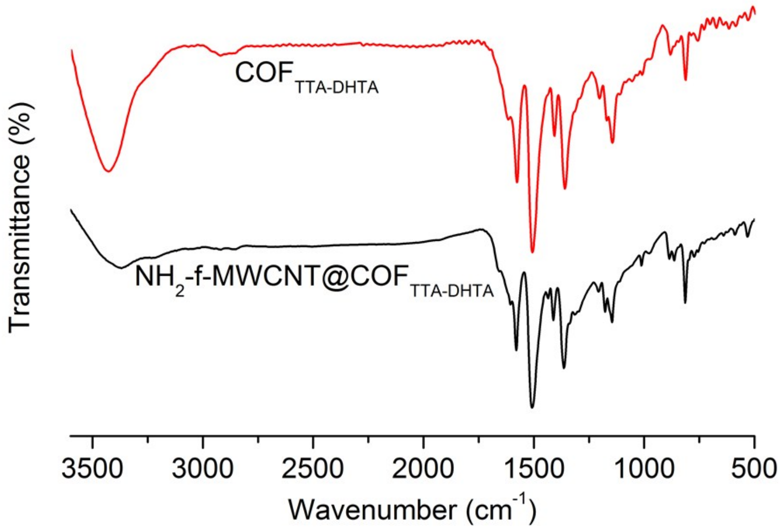

Fig. S6 FT-IR spectra of NH_2-f-MWCNT@COF$_{TTA\text{-}DHTA}$ (black curve) compared to COF$_{TTA\text{-}DHTA}$ (red curve).

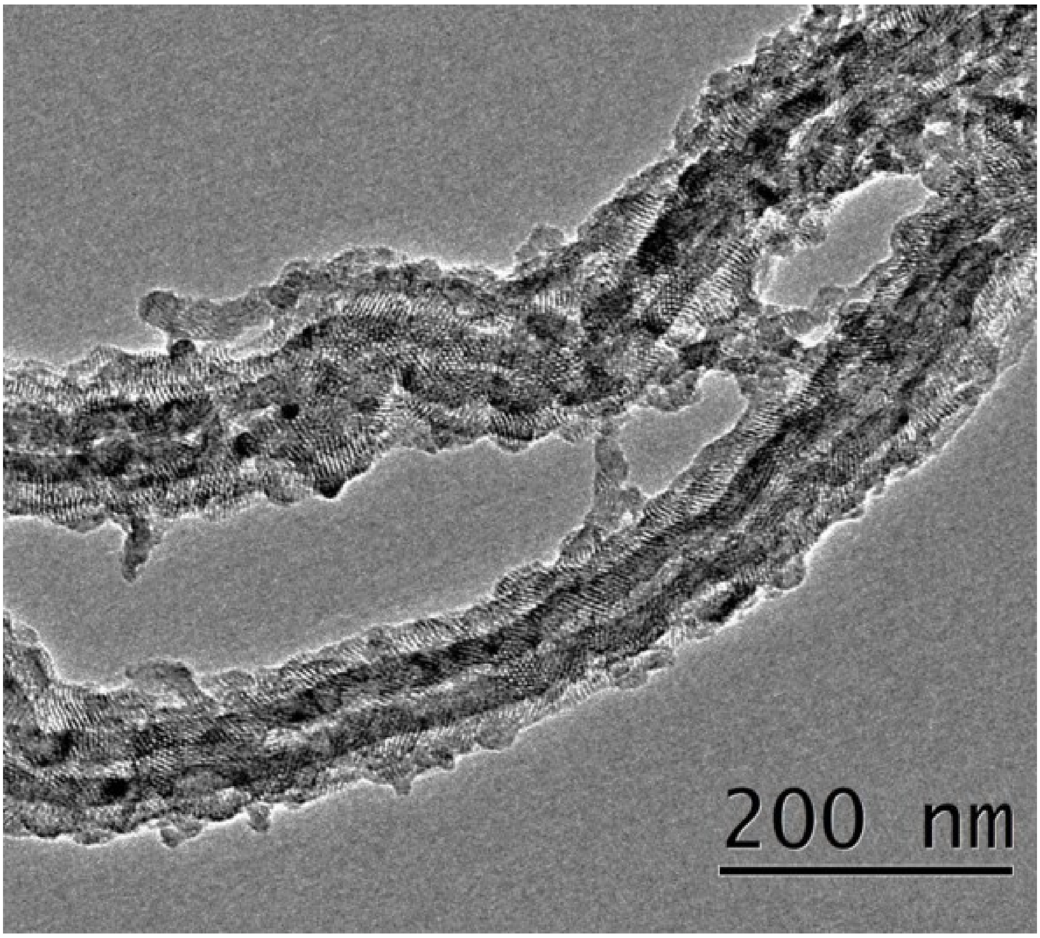

Fig. S7 TEM image of NH_2-f-MWCNT@COF$_{TTA\text{-}DHTA}$ in large scale with the NH_2-f-MWCNT concentration of 10 mg mL^{-1}.

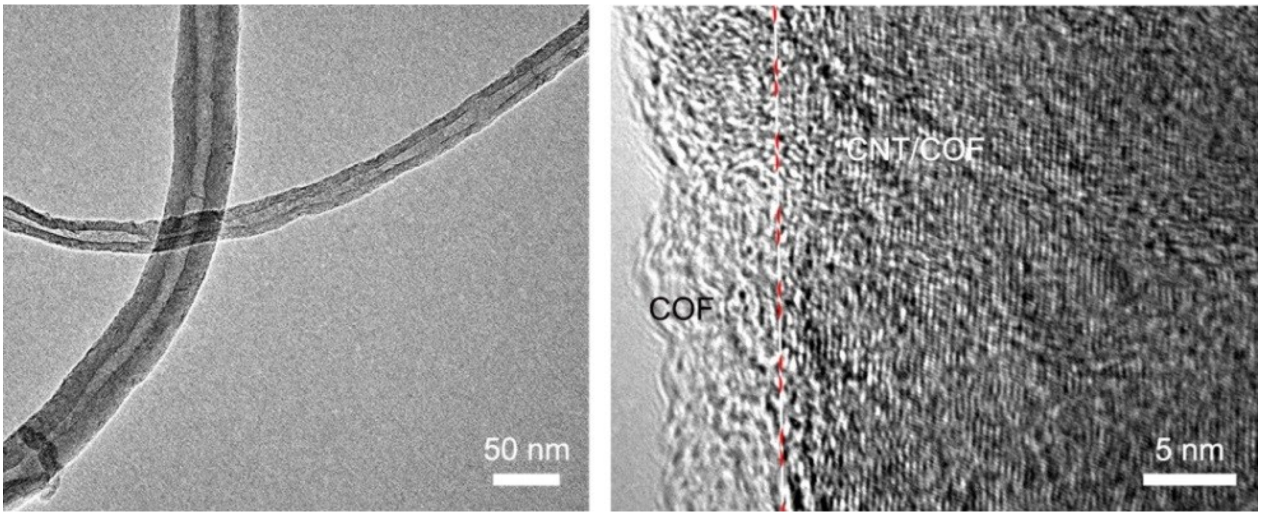

Fig. S8 TEM images of NH_2-f-MWCNT@COF$_{TTA\text{-}DHTA}$ in the case of 20 mg mL^{-1} of NH_2-f-MWCNT in dioxane/mesitylene/DMF.

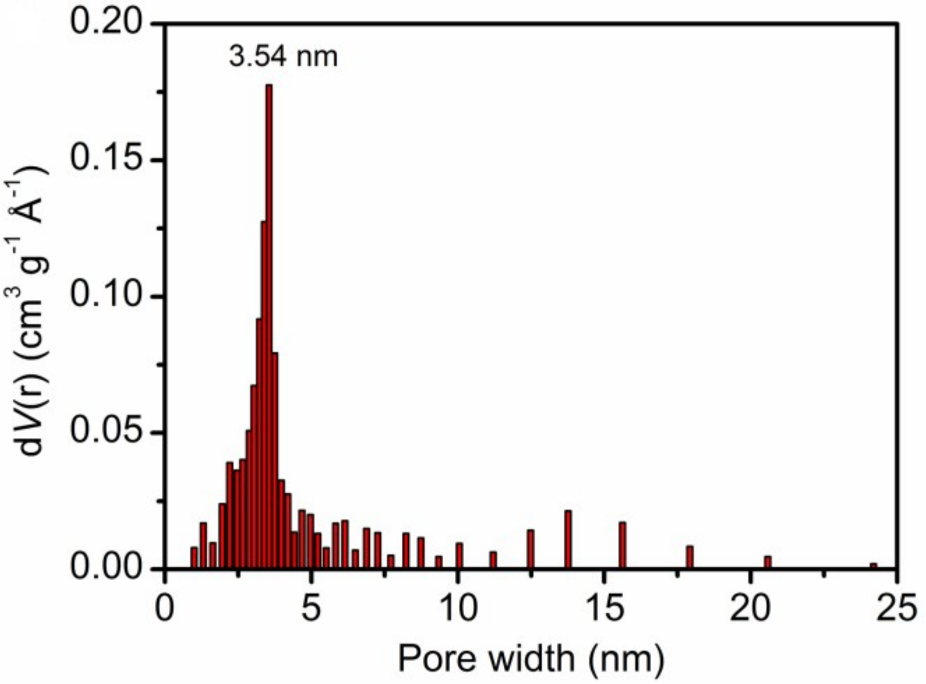

Fig. S9 Pore size distribution of NH_2-f-MWCNT@COF$_{TTA\text{-}DHTA}$. The pore with a size of *ca.* 14.7 nm could be attributed to that of NH_2-f-MWCNT.

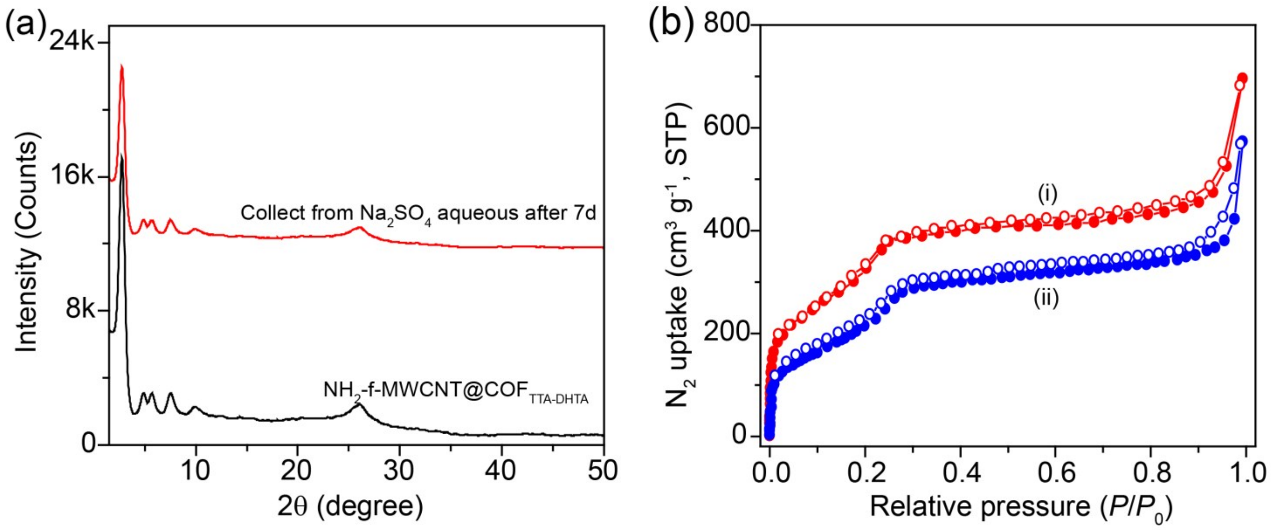

Fig. S10 (a) PXRD patterns of pristine NH$_2$-f-MWCNT@COF$_{TTA-DHTA}$ and collect from 1 M Na$_2$SO$_4$ aqueous solution after 7 days. (b) Nitrogen adsorption isotherms at 77 K for NH$_2$-f-MWCNT@COF$_{TTA-DHTA}$ as freshly synthesized (red circle) and after submerging in 1 M Na$_2$SO$_4$ aqueous solution for 7 days (blue circle).

The high crystallinity of NH$_2$-f-MWCNT@COF$_{TTA-DHTA}$ remains after submerged in 1 M Na$_2$SO$_4$ aqueous solution for 7 days. And the porosity of samples is remained well only with a small decrease of surface area (from 1157 m^2 g^{-1} to 982 m^2 g^{-1}). These results indicate the excellent chemical stability of as-prepared NH$_2$-f-MWCNT@COF$_{TTA-DHTA}$.

S4. Electrochemical measurments

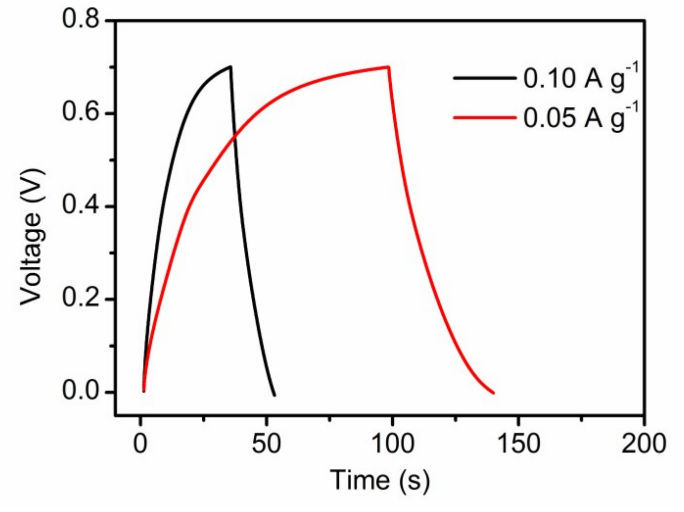

Fig. S11 Galvanostatic charge-discharge curves for $COF_{TTA-DHTA}$.

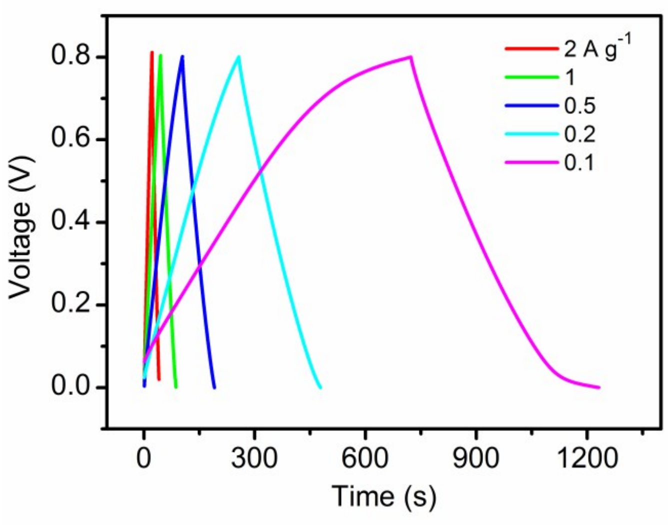

Fig. S12 Galvanostatic charge-discharge curves for NH_2-f-MWCNT.

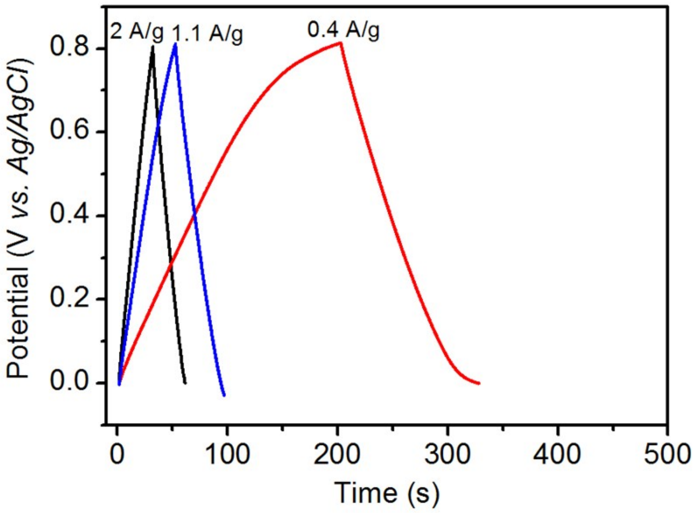

Fig. S13 Galvanostatic charge-discharge curves for MWCNT@ $COF_{TTA-DHTA}$.

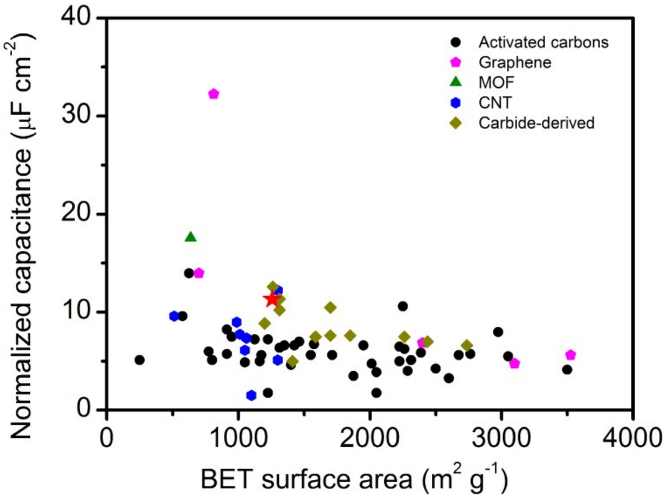

Fig. S14 Comparison of the normalized capacitance of various EDLC materials relative to their BET surface areas.[4-10] Red star represents the result in the present work.

References

1 A. Halder, S. Kandambeth, B. P. Biswal, G. Kaur, N. C. Roy, M. Addicoat, J. K. Salunke, S. Banerjee, K. Vanka, T. Heine, S. Verma and R. Banerjee, *Angew. Chem. Int. Ed.*, 2016, **55**, 7806-7810.

2 J.-i. Kadokawa, Y. Tanaka, Y. Yamashita and K. Yamamoto, *Eur. Polym. J.*, 2012, **48**, 549-559.

3 S. Kandambeth, D. B. Shinde, M. K. Panda, B. Lukose, T. Heine and R. Banerjee, *Angew. Chem. Int. Ed.*, 2013, **52**, 13052-13056.

4 D. Sheberla, J. C. Bachman, J. S. Elias, C. J. Sun, Y. Shao-Horn and M. Dinca, *Nat. Mater.*, 2017, 10.1038/nmat4766.

5 W. Gu and G. Yushin, *Wiley Interdiscip. Rev.: Energy Environ.*, 2014, **3**, 424-473.

6 Y. Zhu, S. Murali, M. D. Stoller, K. J. Ganesh, W. Cai, P. J. Ferreira, A. Pirkle, R. M. Wallace, K. A. Cychosz, M. Thommes, D. Su, E. A. Stach and R. S. Ruoff, *Science*, 2011, **332**, 1537.

7 A. Izadi-Najafabadi, S. Yasuda, K. Kobashi, T. Yamada, D. N. Futaba, H. Hatori, M. Yumura, S. Iijima and K. Hata, *Adv. Mater.*, 2010, **22**, E235-E241.

8 L. Zhang, F. Zhang, X. Yang, G. Long, Y. Wu, T. Zhang, K. Leng, Y. Huang, Y. Ma, A. Yu and Y. Chen, *Sci. Rep.*, 2013, **3**, 1408.

9 Y. Xu, Z. Lin, X. Zhong, X. Huang, N. O. Weiss, Y. Huang and X. Duan, *Nat. Commun.*, 2014, **5**, 4554.

10 X. Yang, C. Cheng, Y. Wang, L. Qiu and D. Li, *Science*, 2013, **341**, 534.